



Elsevier has created a [Monkeypox Information Center](#) in response to the declared public health emergency of international concern, with free information in English on the monkeypox virus. The Monkeypox Information Center is hosted on Elsevier Connect, the company's public news and information website.

Elsevier hereby grants permission to make all its monkeypox related research that is available on the Monkeypox Information Center - including this research content - immediately available in publicly funded repositories, with rights for unrestricted research re-use and analyses in any form or by any means with acknowledgement of the original source. These permissions are granted for free by Elsevier for as long as the Monkeypox Information Center remains active.



# Adamantane derivatives as potential inhibitors of p37 major envelope protein and poxvirus reproduction. Design, synthesis and antiviral activity



Vadim A. Shiryaev<sup>a, \*</sup>, Michael Yu Skomorohov<sup>a</sup>, Marina V. Leonova<sup>a</sup>,  
Nikolai I. Bormotov<sup>b</sup>, Olga A. Serova<sup>b</sup>, Larisa N. Shishkina<sup>b</sup>, Alexander P. Agafonov<sup>b</sup>,  
Rinat A. Maksyutov<sup>b</sup>, Yuri N. Klimochkin<sup>a</sup>

<sup>a</sup> Department of Organic Chemistry, Samara State Technical University, 244 Molodogvardeyskaya St., Samara, Samara Region, 443100, Russia

<sup>b</sup> State Research Centre of Virology and Biotechnology VECTOR, Koltsovo, Novosibirsk Region, 630559, Russia

## ARTICLE INFO

### Article history:

Received 12 March 2021

Received in revised form

13 April 2021

Accepted 15 April 2021

Available online 29 April 2021

### Keywords:

Adamantane

Orthopox viruses

Molecular modelling

Drug design

Antiviral activity

## ABSTRACT

Currently, smallpox, caused by the variola virus belonging to the poxvirus family, has been completely eradicated according to the WHO. However, other representatives of poxviruses, such as vaccinia virus, cowpox virus, ectromelia virus, monkeypox virus, mousepox virus and others, remain in the natural environment and can infect both animals and humans. The pathogens of animal diseases, belonging to the category with a high epidemic risk, have already caused several outbreaks among humans, and can, in an unfavorable combination of circumstances, cause not only an epidemic, but also a pandemic. Despite the fact that there are protocols for the treatment of poxvirus infections, the targeted design of new drugs will increase their availability and expand the arsenal of antiviral chemotherapeutic agents. One of the potential targets of poxviruses is the p37 protein, which is a tecovirimat target. This protein is relatively small, has no homologs among proteins of humans and other mammals and is necessary for the replication of viral particles, which makes it attractive target for virtual screening. Using the I-TASSER modelling and molecular dynamics refinement the p37 orthopox virus protein model was obtained and its was confirmed by ramachandran plot analysis and superimposition of the model with the template protein with similar function. A virtual library of adamantane containing compounds was generated and a number of potential inhibitors were chosen from virtual library using molecular docking. Several compounds bearing adamantane moiety were synthesized and their biological activity was tested *in vitro* on vaccinia, cowpox and mousepox viruses. The new compounds inhibiting vaccinia virus replication with IC<sub>50</sub> concentrations between 0.133 and 0.515 μM were found as a result of the research. The applied approach can be useful in the search of new inhibitors of orthopox reproduction. The proposed approach may be suitable for the design of new poxvirus inhibitors containing cage structural moiety.

© 2021 Elsevier Masson SAS. All rights reserved.

## 1. Introduction

Poxviruses occupy a special place among DNA genomic viruses. The variola virus, which belongs to the genus of orthopoxviruses of the poxviridae family, is considered to be one of the most dangerous viruses because of its pathogenic and epidemic properties (mortality exceeds 30%) and poses a serious threat as a biological agent for bioterrorism [1,2].

Although smallpox is now globally eradicated, the infections caused by zoonotic pox viruses may still be a threat. Monkeypox, cowpox and parapox viruses are already causing outbreaks in humans [3,4]. New zoonotic poxviruses are discovered lately [5]. The increase in the number of people with reduced immunity and the fashion for the maintenance of exotic animals increases the frequency of people contacts with undiscovered animal poxviruses and, therefore, increases the probability of emergence of new

\* Corresponding author.

E-mail address: [shiryaev.va@samgtu.ru](mailto:shiryaev.va@samgtu.ru) (V.A. Shiryaev).

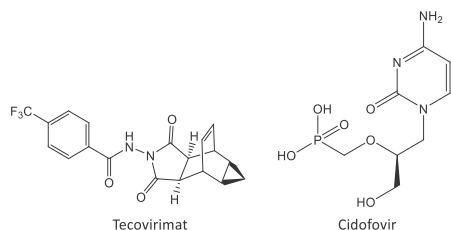
mutant poxvirus strain more pathogenic to humans, that put animal poxviruses in the range of high epidemic risk pathogens.

Moreover, the progress of modern biotechnology opens the way to the creation of genetically modified microorganisms with increased pathogenicity and drug resistance [6]. Since the structure of the poxvirus genome is now well known, there is a danger of creating an artificial poxvirus pathogen [7,8].

Poxviruses are the largest and the most complex of all known human and animal viruses. Their genome is represented by double-stranded DNA, which contains information on the amino acid sequence of several dozen polypeptides. The reproductive cycle of the smallpox virus is very complex. The processes of poxvirus maturation and exit from the cell, as well as the processes of penetration into the cell, are multistage and include intermediate stages [9,10].

Variability and mutation of viruses as well as the possibility of the emergence of new mutagenic forms on the one hand, and the limited arsenal of antiviral agents on the other, necessitate the search for new effective antiorthopoxvirus agents.

Anti-smallpox activity has been found among a wide range of cage compounds [11–13]. Screening of a huge number of cage compounds revealed a number of promising drug candidates with pronounced antiviral activity. Inhibitors of orthopoxvirus reproduction have been found in the series of functionalized compounds containing adamantane moiety [14–23].



Currently one of the most effective drugs against orthopoxviruses is 4-trifluoromethyl-N-(3,3a,4,4a,5,5a,6,6a-octahydro-1,3-dioxo-4,6-ethenocyclop[*f*]isoindole-2-(1H)-yl)benzamide (Tecovirimat, ST-246) [24–26].

This drug, found by SIGA Technologies (USA), is effective against a number of orthopoxviruses, including vaccinia virus, monkeypox viruses, cowpox, camelpox and ectromelia virus and now is approved by FDA (“Tpoxx”) for treatment of adult and pediatric patients infected with variola virus [27].

The mechanism of action of tecovirimat is related to the formation of enveloped forms of orthopoxviruses. It prevents the wrapping of virion and so dramatically decreases the rate of spreading of viruses in the tissue. The protein, that is believed to be affected by tecovirimat, is a relatively small globular peripheral membrane protein weighing 37 kDa (p37) that plays a central role in the envelopment viral particles and is coded by a highly conserved F13L gene [28] and has no mammalian homologs. The viruses bearing artificially mutated variant of this gene were up to 10000 times less sensitive to tecovirimat comparing to wild type strain [29]. Purified p37 shows lipase activity [30,31], however the actual role of lipase activity in p37 function is unclear and may involve p37-induced membrane alterations [31,32]. Several investigations evidence that p37 interacts with host cellular membrane proteins Rab9 and TIP47. The tecovirimat may disrupt such interactions preventing the formation of intracellular mature virus [33]. The interaction of tecovirimat with p37 protein in is under no hesitance [34], however the exact mechanism of interruption of reproduction cycle of orthopox viruses by ST-246 is still not investigated.

Taken together, these results validate p37 as potential target for

antiviral drug design.

Since the compounds [14–23] containing the adamantane core frequently exhibit noticeable activity against poxviruses and the adamantane fragment is highly similar in geometry and lipophilicity to the cage fragment tecovirimat, we propose a number of compounds based on the replacement of the hydrocarbon moiety of tecovirimat with the adamantane residue.

## 2. Results and discussion

### 2.1. Design approach

Similarly to design of viral reproduction influenza viruses [35] and hepatitis virus [36] we used the standard approach [37], that includes the molecular modelling of spatial structure of target protein by the means of molecular dynamics, the determination of potential ligands using molecular docking, verification of potential inhibitor by evaluation of biological activity.

To date only primary structure of p37 protein is determined experimentally, as far as secondary and tertiary structures are not investigated. The search for the structure of this protein gave no experimental models and only several primary structures of several strains in the UniProt database. The tertiary models of these proteins are available through SWISS-MODEL Repository basing on PDB structures 4urj and 4ggj or ModBase database basing on PDB structure 1v0w. The SWISS-MODEL is only fragmentary as far as each of the templates are at least twice smaller than p37 protein. On the other side, the ModBase model is based on a homologous *Streptomyces* phospholipase D [28] and its sequence almost fully covers the sequence of p37, however this model is rather outdated.

We have chosen the sequence of protein P20638 (F13\_VACCC) from the UniProt database corresponding to the available experimental vaccinia model. Since the available models of p37 are unconfident, we used blind modelling of p37 protein structure by I-TASSER web service without any predefined templates [38–40]. In these conditions I-TASSER searches the best alignment of proteins through the whole RCSB PDB database. The resulting 3D model is constructed by clustering a large ensemble of similar proteins structural conformations. The confidence and folding of the model are evaluated by C-score and TM-score. The resulting model is characterized by high C-score (0.63) what confirms the high quality of the model. TM-score shows similarity in folding between two or more proteins while low values of TM-score usually appear for randomly chosen structures. The high value of TM-score ( $0.80 \pm 0.09$ ) for predicted model shows good folding, similar to selected templates. The resulting model has very close TM scores and rather small RMSD comparing to the existing experimental models of phospholipase D from *Streptomyces* sp. (1v0w, TM 0.98, RMSD 1.97) what correlates with the lipase activity of p37. The modelling of molecular dynamics (MD) was used to refine the predicted model in order to remove the steric clashes of the residues and to check the stability of the protein during thermal motion. The initial model for MD simulation was constructed using CHARMM-GUI web service [41–43]. At the first stage, the protein was palmitoylated on Cys185 and Cys186 residues [44], introduced into 1-palmitoyl-2-oleoyl-*sn*-glycero-3-phosphocholine (POPC) bilayer and solvated with water containing  $K^+$  and  $Cl^-$  ions with a concentration of 0.15 M. As far as no complexes of similar proteins with metals are known, but on the contrary metal-free complexes of substrates exist (for example 1v0w), no other ions were introduced into the system. Next, the structure was optimized at 310 K with restraints on the movement of protein backbone and side chains using NAMD software [45]. Then the resulting structure underwent a stage of equilibration at a time interval of 80 ns at 310 K. The analysis of RMSD during equilibration showed, that the

protein reached equilibrium in 40 ns and the further calculation was carried out to improve reliability of the model.

The last 40 ns (40–80 ns interval, 4000 snapshots with 10 ps increment) of molecular dynamics trajectory was analysed with Chimera [46] and all snapshots were clustered basing on the mass-weighted RMSD of the heavy atoms (see Fig. 1). The representative frameshots of 10 most populated clusters were chosen for virtual screening in order to increase the reliability of molecular docking. The reliability of every model was validated by analyzing its ramachandran plot and determination of compatibility of 3D model with its sequence by Verify 3D and PROCHECK service [47] (Fig. 2).

The distributions of  $\phi$  (psi) and  $\psi$  (phi) of the amino acid residues obtained by ramachandran plots showed that 84.9% were in most favoured regions, 10.7% in additional allowed region and 3.6% in generously allowed region. Only 3 residues (0.9%) were in disallowed region, which are Cys185, Ser207 and Ile195 which can be caused by proximity of lipid layer to these residues as Cys186 and Cys186 are palmytoilated and act as anchor residues. The quality of the model was also qualified by superimposition the XRD structure of phospholipase 1v0w with modelled protein. As seen on Fig. 3 almost all helices, sheets and binding sites are overlapping among these structures.

The binding site of most phospholipases D, which are similar to p37, is known to be situated within the HKD domains that is highly conserved among all phospholipases [48]. As a result, these domains catalyzes the hydrolysis of phospholipids. The prediction of binding site with COFACTOR module of I-TASSER gave the most probable binding site similar to the phospholipase 1v0r with the C-score 0.29. The residues that form the site are Phe52, Leu118, Cys120, Ser135, Asn312, Lys314, Asn329 and Asp331. To define other possible pockets we conducted a blind docking of the known smallpox replication inhibitor tecovirimat within the whole protein using the AutoDock Vina software [49].

Five potential binding sites were found with the binding energies of tecovirimat ranged from  $-6.1$  to  $-9.3$  kcal/mol. However, the best cavity was the same as predicted by COACH with a calculated binding energy to protein  $-9.3$  kcal/mol, which is 1.5 kcal/mol lower than the next rated cavity.

The validation of docking modes of tecovirimat was performed by simulation of molecular dynamics of ST-246 and p37 complex for 80 ns. The procedure of building the starting model and simulation parameters was the same as in modelling the lone protein. The analysis of RMSD shows that the complex retains for the whole time of simulation and reaches equilibrium after 60 ns of simulation (Fig. 4). The simulation of molecular dynamics for complexes of p37 with ST-246 in other cavities but all of them were unstable and dissociate at time interval 10–20 ns (see Fig. 5).

## 2.2. Virtual screening of potential p37 inhibitors

In order to find new potential inhibitors of poxvirus replication, we constructed a number of compounds containing adamantane pharmacophore residue and a fragment of 4-substituted benzoic acid that have structural similarity with the known active compounds — tecovirimat. The selection of *p*-bromo and *p*-trifluoro substituents is governed by the empiric dependencies of antiviral activity from electronegativity of substituent [50]. The results of the research showed that electron donating groups at 4- position as well as electron withdrawing groups at 2- position increases the EC<sub>50</sub> of compound, whereas electron withdrawing groups at 3- and 4- positions decreases EC<sub>50</sub>. The most active compounds contained 4-Br and 4-CF<sub>3</sub> substituted benzene ring. Adamantane cage was chosen because of its spatial similarity to tecovirimat cage fragment. While the Van de Waals volume of adamantane ( $124.5 \text{ \AA}^3$ ) is slightly bigger than tecovirimat cage fragment ( $109.79 \text{ \AA}^3$ ), the

VdW volume of other available cage fragments is either smaller, for example bicyclo[2.2.2]octane ( $101.5 \text{ \AA}^3$ ), or noticeably bigger, for example bornane ( $138.8 \text{ \AA}^3$ ). At the same time adamantane and tecovirimat cage have very similar VdW areas ( $131.7 \text{ \AA}^2$  and  $124.0 \text{ \AA}^2$  respectively). Thus, the presence of adamantane moiety in the structure of the ligand increases the probability of suitable binding of ligand to p37. Therefore, we decided to construct a set of virtual compounds, containing structural fragments using ACD Labs Chem Sketch software pack [51].

The geometry of virtual structures was optimized using the molecular mechanics method in the MMFF94 force field using the Avogadro 1.1.1 molecular editor [52]. The docking of a set of structures to the p37 protein cavity revealed 19 compounds that are promising for further research and optimization by varying their structure. The structures of ligands, which showed the best binding energy for protein p37 and their average values (kcal/mol), calculated using Autodock Vina, are shown in Table 1.

The analysis of docking results was performed with Discovery Studio software package [53] and showed interactions of ligands with Phe25, Tyr150, Asn312, Lys314 and Phe307 for both tecovirimat and proposed ligands. Moreover all ligands are positioned in the cavity of protein similarly: the lipophilic hydrocarbon cage of the molecule directed towards Phe307, trifluoromethyl group directed to Lys314 and Asn312 and carbonyl group directed to Asp361.

However, it should be noted, that all chosen structures have close calculated affinities that are rather moderate. The most likely cause of this phenomenon is rather big volume of cavity that binds the ligand. The spatial structure of the protein allows the ligands with close steric properties to enter the binding site and interact with amino acid sidechains that directed into the cavity. On the other side, the binding site is not very deep, therefore ligands are not encapsulated by protein and remain rather agile, what can explain moderate binding energies. According to the results of molecular docking we decided to build a model of pharmacophore of the present protein. The best binding modes of the most active compounds were submitted to PharmGist [54,55] web service which produced the spatial dislocation of several features. The average throughout the whole set of ligands dislocation of molecular features are shown in Fig. 6: the bulky hydrocarbon cage (white) should be linked to aromatic ring (blue) by a linker, containing H-bond donors and acceptors (magenta).

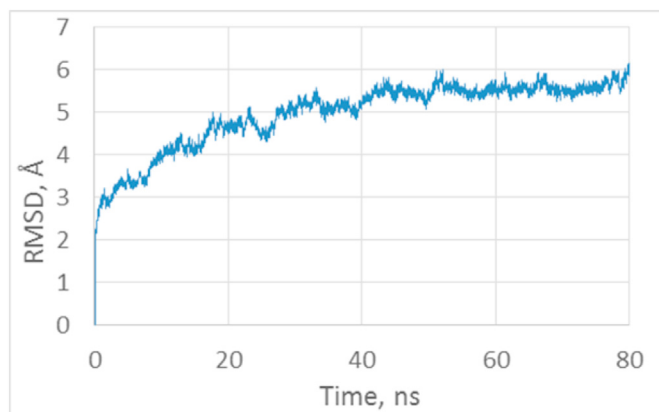


Fig. 1. RMSD of p37-POPC bilayer complex during production stage of molecular dynamics.

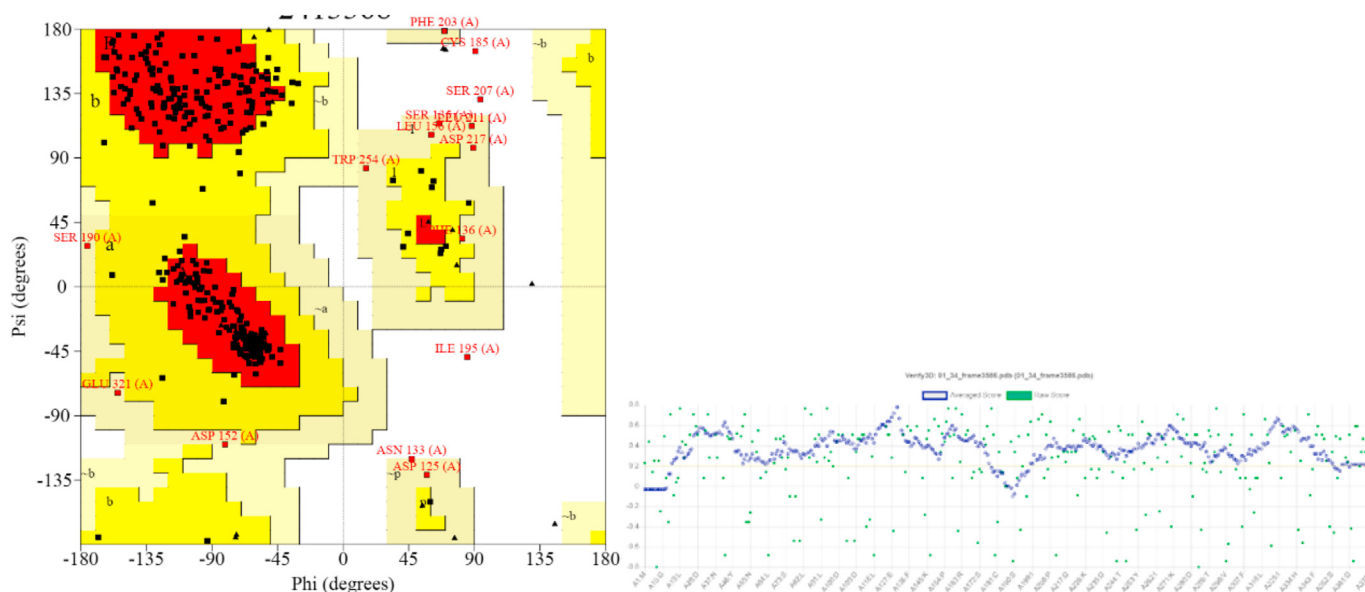


Fig. 2. Ramachandran plot and results of Verify\_3D analysis of p37 model.



Fig. 3. Superimposition of modelled p37 (light blue) and phospholipase 1v0w. The binding site of both proteins is shown by yellow sphere.

### 2.3. Organic synthesis

Twenty compounds with the best binding were synthesized for determination their antiviral activity. The N-adamantylated aryl-carboxamides **5–9**, **11**, **12** were obtained by acylation of the amines of the adamantane series **1–4**, **10** with benzoyl chlorides, containing electron-withdrawing substituents in the para-position (Scheme 1). The corresponding benzhydrazides **16–18** were synthesized by the reaction of adamantancarboxylic acids hydrazides **13–15** with *p*-trifluoromethylbenzoyl chloride (Scheme 2). Reaction of 1-adamantylsemicarbazide **19** with *p*-trifluoromethylbenzoyl chloride gave N-(adamantan-1-yl)-2-(4-(trifluoromethyl)benzoyl)hydrazin-1-carboxamide **20**.

Hydrazones of the adamantane series **25**, **26**, **31** were synthesized from the corresponding ketones — 2-adamantanone **21**, 5-chloro-2-adamantanone **22** and 1-(adamantan-1-yl)ethan-1-one

**29** by reaction with hydrazine hydrate and the subsequent acylation of the compounds obtained with *p*-trifluoromethylbenzoyl chloride. The corresponding benzhydrazides **27**, **28**, **32** were obtained by reduction of hydrazones **25**, **26**, **31** with sodium cyanoborohydride in methanol (Scheme 3).

The corresponding benzhydrazides **35**, **36** were obtained from 1-adamantylhydrazines **33**, **34** and *p*-trifluoromethylbenzoyl chloride (Scheme 4).

The data of the extensive testing of compounds showed that the activity spectrum of most compounds extends to a wide range of orthopoxviruses, pathogenic for humans. At the same time, various representatives of orthopoxviruses differ in sensitivity to the same drug. One can trace the tendency that the cowpox virus has the least sensitivity to the antiviral compounds studied than the vaccinia virus (Table 1).

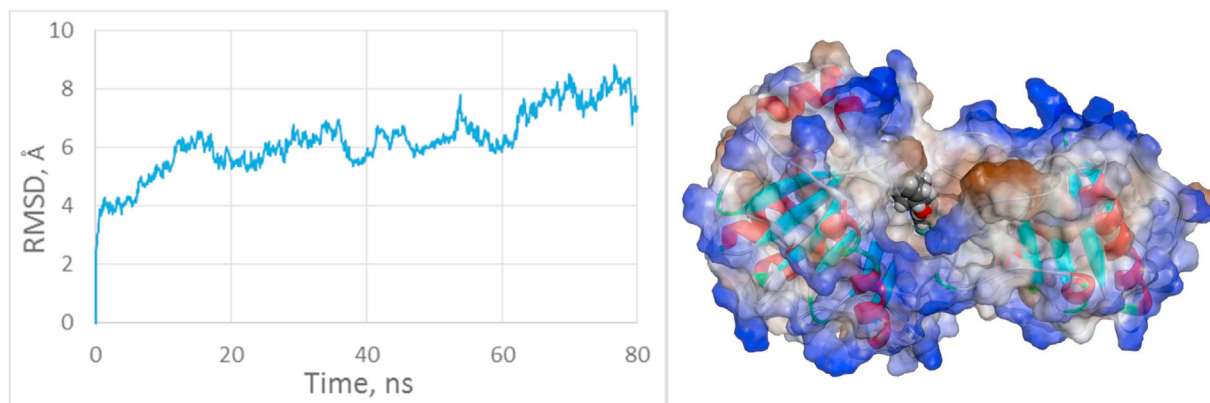
Basing on the results obtained, it can be assumed that the trifluoromethylbenzamides **5**, **8** and **12** are the most promising for further *in vitro* and *in vivo* studies. The effective concentration of N-(1-adamantyl)-4-trifluoromethylbenzamide **5** against vaccinia virus is 0.133  $\mu\text{M}$ , while the cytotoxic activity is more than 309  $\mu\text{M}$  therefore the value of the selectivity index (CC50/IC50 ratio) of **5** is more than 2325. Also, the compound **5** effectively suppresses the reproduction of mousepox virus at a concentration of 0.492  $\mu\text{M}$  (selectivity index is more than 628) and cowpox virus at a concentration of 0.928  $\mu\text{M}$  (SI = 333).

Compound **8** effectively inhibit reproduction of vaccinia virus at concentration of 0.27  $\mu\text{M}$  and selectivity index more than 1098. In addition, benzamide **8** showed effectiveness against cowpox virus at a concentration of 1.24  $\mu\text{M}$  (SI > 239). However, benzamide **8** did not show a virus inhibitory effect on the mousepox virus.

Trifluoromethylbenzamide **12** showed effectiveness against vaccinia, mousepox and cowpox viruses. The effective concentration of **12** against vaccinia virus is 0.216  $\mu\text{M}$ , while the cytotoxic activity is more than 309  $\mu\text{M}$  and the selectivity index is 1428. Compound **12** inhibits reproduction of mousepox virus at a concentration of 0.569  $\mu\text{M}$  (SI > 543) and cowpox virus at a concentration of 0.960  $\mu\text{M}$  (SI > 321).

According to the data acquired it should be noted that the presence of alkyl groups at adamantyl cage or at side chain leads to recession of antiviral activity and elevation of cytotoxicity. The





**Fig. 4.** RMSD of p37 – ST-246 – POPC complex during production stage of molecular dynamics (left) and the view of the complex (right). The surface of the protein is colored according to residues hydrophobicity from brown (hydrophobic) to blue (hydrophilic), ST-246 is represented by spacefill model.

replacement of trifluoromethyl group by bromine also leads to decrease in inhibitory activity.

It can be noticed, that despite all chosen compounds have close computed binding energies, their evaluated biological activities vary a lot. Whereas the best compound **5** is only 50 times less active than the reference compound – tecovirimat, the worst is totally inactive. The most probable reason of this phenomenon the complexity of interaction of a compound with the whole cell comparing to isolated protein. The other explanation of the observed phenomena may be the interaction between p37 and other membrane proteins or covalent interaction between five membered imide ring and active site of p37 that cannot be easily modelled by means of molecular dynamics. However, the proposed procedure can still be useful. As far as the first stage of inhibition of a target protein includes formation of simple complex, primarily by van der Waals forces and hydrogen bonds, and consequent formation of covalent bond may occur only on the next stage, the application of molecular docking can distinguish the potential binding molecules from those that can not achieve the binding site of p37.

### 3. Conclusion

In summary, using methods of virtual modelling, we have acquired a model of p37 orthopoxvirus membrane protein that can be

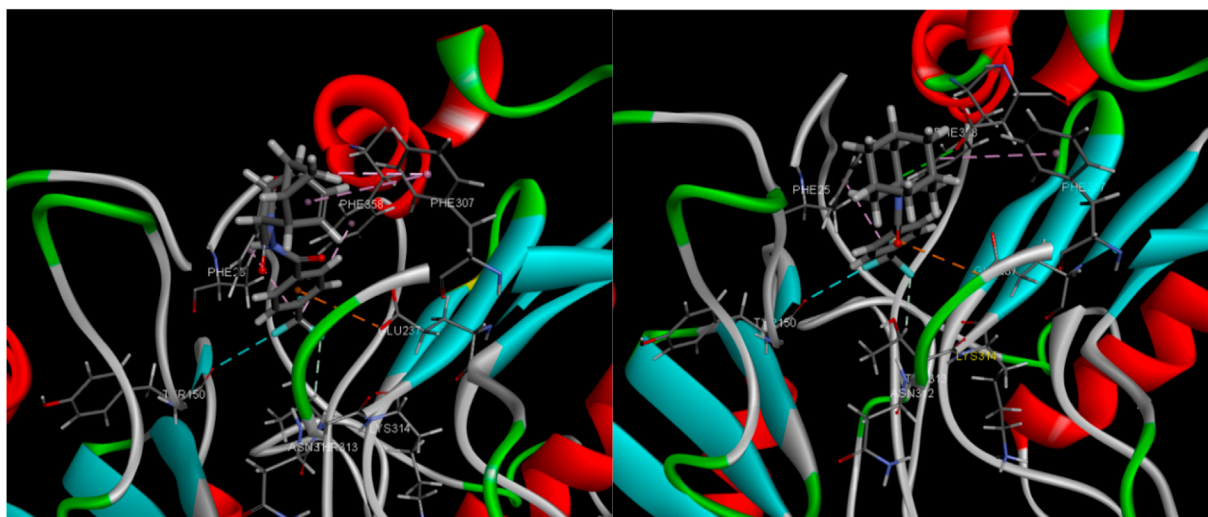
used for further development of new inhibitors of orthopoxvirus reproduction by means of molecular docking. A series of adamantane-containing compounds have been synthesized and their antiviral activities against vaccinia, cowpox and mousepox viruses were defined *in vitro*. Although the results of molecular docking do not show good correlation with experimental data, probably due to complex interactions between p37 and other viral and host proteins or drug-like molecules with lipophilic cell membranes in native conditions, it still allows to reveal compounds with high potential activities *in vitro*. In the structure of poxvirus replication inhibitors the three main structural fragments can be distinguished - a lipophilic cage residue and a fragment of a benzene linked together by a hydrophilic fragment.

The discovery of several compounds, which  $IC_{50}$  lies in sub-micromolar range, indicates that adamantane scaffold has considerable potential for creating new effective antiorthopoxvirus drug candidates and there is an opportunity of finding such compounds among tecovirimat analogues with different hydrocarbon cage type.

### 4. Experimental

#### 4.1. Protein modelling and virtual docking

The initial protein sequence was obtained from the UniProt



**Fig. 5.** The residues of p37 interacting with **5** (left) and tecovirimat (right) acquired by molecular docking. Visualized with Discovery Studio.

**Table 1**  
Cytotoxicity, antiviral activity against orthopoxviruses (vaccinia, cowpox and mousepox viruses) and calculated binding affinities of compounds.

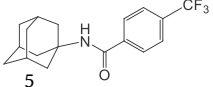
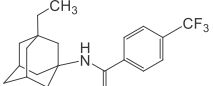
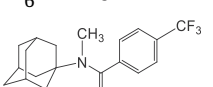
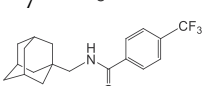
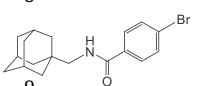
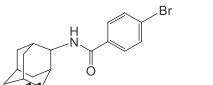
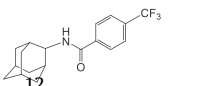
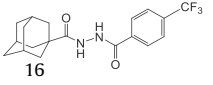
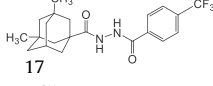
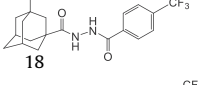
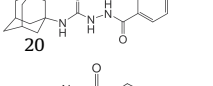
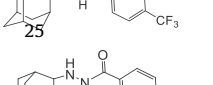
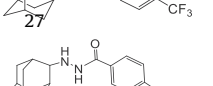
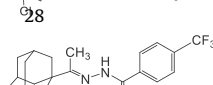
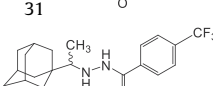
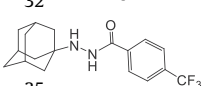

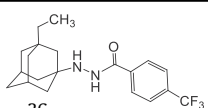
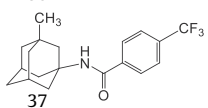
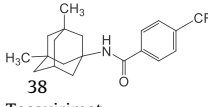
Compounds	CC50 ( $\mu\text{M}$ )	IC50 ( $\mu\text{M}$ )/SI (CC50/IC50)			Binding affinity (Vina, kcal/mol)
		Vaccinia	Cowpox	Mousepox	
	>309.3	<b>0.133/&gt;2325</b>	0.928/>333	0.492/>628	-8.1
	>280	4.1/>68	11.06/>25	11.1/>25	-8.4
	>296.4	4.85/>61	32.9/>9	6.17/>48	-8.1
	>296.4	<b>0.27/&gt;1098</b>	1.24/>239	n/a	-8.3
	238	8.3/28	n/a	1.75/136	-7.5
	>299.2	3.06/>98	11.3/>26.5	4.9/>61	-7.2
	>309	<b>0.216/&gt;1428</b>	0.96/>321	0.569/>543	-7.9
	>273	1.07/>255	4.77/>57	1.0/>273	-8.8
	>253.7	30.9/>8.2	n/t	n/t	-9.1
	47	12.53/3.75	n/a	n/a	-9.0
	94.3	36.26/2.6	n/t	n/t	-9.1
	>297	198/>1.5	n/t	n/t	-8.6
	>296	2.8/>103	4.06/>72	2.5/>118	-8.4
	~214.6	3.52/61	10.36/20.7	7.8/27.5	-8.5
	>274.4	10.55/>26	11.9/>23	10.9/>25	-8.7
	14	<b>0.515/27</b>	n/t	n/t	-8.8
	2.8	n/a	n/t	n/t	-8.4

Table 1 (continued)

Compounds	CC50 ( $\mu\text{M}$ )	IC50 ( $\mu\text{M}$ )/SI (CC50/IC50)			Binding affinity (Vina, kcal/mol)
		Vaccinia	Cowpox	Mousepox	
	2.5	1.66/1.5	n/t	n/t	-8.7
	>296.4	8.98/>33	15.6/>19	4.1/>72	-8.4
	20.5	n/a	n/t	n/t	-8.4
Tecovirimat	>266	0.00266/>100000	0.00532/>50000	0.00806/>33000	-8.9

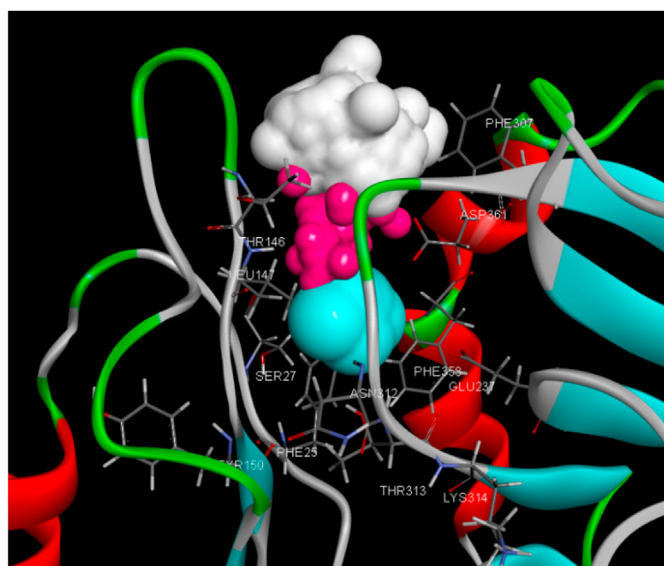
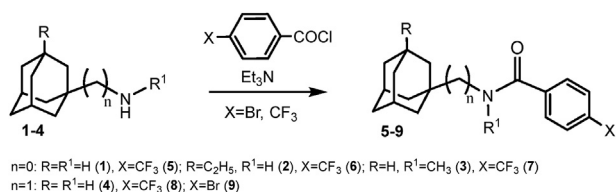
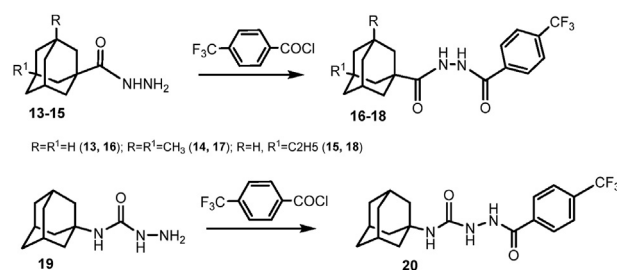


Fig. 6. The pharmacophore model of p37 inhibitors.

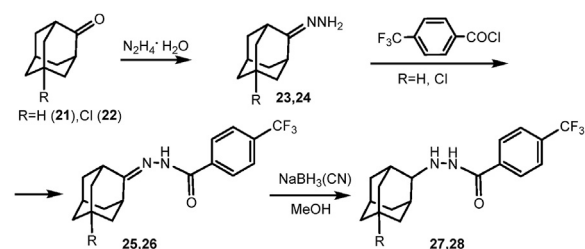


Scheme 1. Synthesis of compounds 5–9, 11, 12.

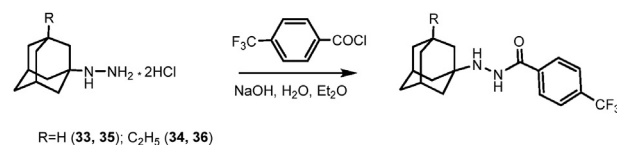
database P20638 (F13\_VACCC). The I-TASSER web service was used to model the initial tertiary structure [38–40]. The obtained model proceeded the stage of refinement by molecular dynamics simulation at neutral pH. The initial model was achieved by CHARMM-GUI web service input generator [41–43]. The protein was palmitoylated on Cys185 and Cys186 residues, integrated into POPC



Scheme 2. Synthesis of compounds 16–18, 20.



Scheme 3. Synthesis of compounds 25–28, 31, 32.



Scheme 4. Synthesis of compounds 35, 36.

bilayer and embedded into rectangular periodic boundary box with walls at least 20 Å away from the sides of the protein. The box was infilled with water molecules (TIP3P model) and some of them were replaced by chlorine and potassium ions to ensure electric



neutrality and KCl concentration of 0.15 M. The resulting system contained about 100,000 atoms.

The molecular dynamics simulations were performed by NAMD 2.11 package using NVIDIA CUDA acceleration on two NVIDIA GeForce GTX 1080 GPUs [45]. The CHARMM36 force field was used for protein [56,57]. The initial minimization included 10000 steps of steepest descent following equilibrating step of 25 ps using Langevin thermostat at 310 K and Langevin barostat at 1.013 kPa. The integration step value was 2 fs in combination with rigid Bonds/SHAKE algorithm. The production step included 40 ns of molecular dynamics at 1.013 kPa and 310 K using Langevin barostat and thermostat.

The analysis and visualization of the results was performed with UCSF Chimera package [46]. The last 40 ns of production step were clustered basing on cross-pair RMSD values of protein backbone atoms. The resulting pattern contained 40 clusters, the representing frames from 10 the most populated of which were chosen for next stage of virtual screening.

The library of potential ligand structures was prepared using the ACD ChemSketch 2015 software [51] and their geometries were optimized with molecular mechanics in the MMFF94 force field using Avogadro 1.2.0 [52]. The PDB files were converted to the PDBQT format using the AutoDock Raccoon 1.0 software [58].

The p37 protein models were prepared for molecular docking using the AutoDockTools 1.5.6 software [59]. First the chosen models were cleared from water and ions and the grid box was set to cover the entire protein. The docking was performed with exhaustiveness set to 1000 and number of modes to 50. The resulting binding modes divided into several groups. The area occupied by the group with the lowest binding energies was considered as binding site. Next the grid box size of approximately  $18 \times 28 \times 16 \text{ \AA}$  was specified in order to cover the entire binding site. Molecular docking was performed using the AutoDock Vina 1.1.2 software [49] with exhaustiveness 1000 and number of modes 50. The analysis of molecular docking results was performed with Discovery Studio Visualiser (free version) [53]. The best calculated affinities were averaged through 10 frames and the best compounds were chosen using energy cut-off of  $-7.2 \text{ kcal/mol}$ .

## 4.2. Chemistry

### 4.2.1. General information

Starting materials and solvents were purchased from commercial suppliers and were used without further purification. The infrared spectra were recorded in potassium bromide disks on Shimadzu IRAffinity-1 FT IR spectrometer. The  $^1\text{H}$  and  $^{13}\text{C}$  NMR spectra (400 and 100 MHz, respectively) were recorded on JEOL-ECX 400 spectrometer using the residual signal of deuterated solvent as internal standard. Chemical shifts are given in ppm; multiplicities are described as singlet (s), doublet (d), triplet (t), quartet (q), multiplet (m) and broad (br); coupling constants are given in Hertz (Hz). Mass spectra were recorded on a GC-mass ThermoFinnigan DSQ spectrometer (70 eV), a quartz column DB-5MS  $30 \text{ m} \times 0.32 \text{ mm}$ , column temperature  $80\text{--}340 \text{ }^\circ\text{C}$  ( $20 \text{ }^\circ\text{C/min}$ ). Elemental analyses were carried out on CHNS-EuroVector EA-3000 EA analyzer with L-cystine as a standard. Melting points were determined on the SRS OptiMelt MPA100 apparatus.

Compounds **33**, **34**, **37**, **38** were synthesized according to known methods [60,61].

### 4.2.2. General procedure for the synthesis of compounds 5–9, 11, 12, 16–18, 20

A solution of 4-X-benzoyl chloride (X = Br,  $\text{CF}_3$ ) (12 mmol) in chloroform (5 mL) was added dropwise to a mixture of amino derivative of adamantane **1–4** or carboxylic acid hydrazide **13–15** or

hydrazinecarboxamide **19** (12 mmol) and triethylamine (15 mmol) in chloroform (6 mL) at  $10 \text{ }^\circ\text{C}$  and the mixture was stirred for 2–3 h at r.t. The resulting solution was evaporated, and the residue was filtered off and washed with cold chloroform, dried and finally recrystallized from ethanol to give (59–72%) the product.

*N*-(Adamantan-1-yl)-4-(trifluoromethyl)benzamide (**5**). Colorless crystals; yield 72%; mp  $159\text{--}160 \text{ }^\circ\text{C}$  (lit.  $160\text{--}161 \text{ }^\circ\text{C}$  [62]). MS,  $m/z$  (%): 323 ( $\text{M}^+$ , 44), 304 (8), 280 (3), 266 (76), 230 (5), 173 (100), 145 (64).

*N*-(3-Ethyladamantan-1-yl)-4-(trifluoromethyl)benzamide (**6**). Colorless crystals; yield 70%; mp  $125\text{--}127 \text{ }^\circ\text{C}$ . IR ( $\nu_{\text{max}}$ ,  $\text{cm}^{-1}$ ): 3356 (N-H), 2910, 1639 (C=O), 1541 (N-H), 1307, 1157, 1126, 1068.  $^1\text{H}$  NMR (DMSO- $d_6$ ),  $\delta$ , ppm: 0.74 (t,  $^3J = 7.6 \text{ Hz}$ , 3H), 1.10 (q,  $^3J = 7.6 \text{ Hz}$ , 2H), 1.34–2.06 (m, 14H), 7.75 (d,  $^3J = 8.2 \text{ Hz}$ , 2H), 7.85 (br. s, 1H), 7.92 (d,  $^3J = 8.2 \text{ Hz}$ , 2H).  $^{13}\text{C}$  NMR (DMSO- $d_6$ ),  $\delta$ , ppm: 7.51, 29.60, 34.45, 36.11, 36.19, 40.88, 40.97, 45.57, 53.16, 124.53 (q,  $^1J_{\text{CF}} = 270.8 \text{ Hz}$ ), 125.52 (q,  $^3J_{\text{CF}} = 3.8 \text{ Hz}$ ), 128.79, 131.19 (q,  $^2J_{\text{CF}} = 31.5 \text{ Hz}$ ), 140.24, 165.46. MS,  $m/z$  (%): 351 ( $\text{M}^+$ , 26), 322 (8), 294 (68), 266 (12), 173 (100), 145 (52). EA calcd. for  $\text{C}_{20}\text{H}_{24}\text{F}_3\text{NO}$ : C 68.36, H 6.88, N 3.99; found: C 68.32, H 6.93, N 4.07.

*N*-(Adamantan-1-yl)-*N*-methyl-4-(trifluoromethyl)benzamide (**7**). Light yellow crystals; yield 61%; mp  $156\text{--}158 \text{ }^\circ\text{C}$ . IR ( $\nu_{\text{max}}$ ,  $\text{cm}^{-1}$ ): 2910, 1693 (C=O), 1622, 1514, 1319, 1120, 1101, 1062.  $^1\text{H}$  NMR (DMSO- $d_6$ ),  $\delta$ , ppm: 1.58–2.26 (m, 15H), 2.71 (s, 3H), 7.84 (d,  $^3J = 8.2 \text{ Hz}$ , 2H), 8.10 (d,  $^3J = 8.2 \text{ Hz}$ , 2H).  $^{13}\text{C}$  NMR (DMSO- $d_6$ ),  $\delta$ , ppm: 29.83, 34.33, 36.51, 38.87, 57.78, 124.48 (q,  $^1J_{\text{CF}} = 271.4 \text{ Hz}$ ), 126.15 (q,  $^3J_{\text{CF}} = 3.8 \text{ Hz}$ ), 130.65, 132.98 (q,  $^2J_{\text{CF}} = 32.4 \text{ Hz}$ ), 135.17, 166.75. MS,  $m/z$  (%): 337 ( $\text{M}^+$ , 97), 318 (7), 280 (100), 186 (10), 173 (70), 145 (44), 135 (70), 107 (6), 93 (12), 79 (12). EA calcd. for  $\text{C}_{19}\text{H}_{22}\text{F}_3\text{NO}$ : C 67.64, H 6.57, N 4.15; found: C 67.59, H 6.65, N 4.11.

*N*-((Adamantan-1-yl)methyl)-4-(trifluoromethyl)benzamide (**8**). Colorless crystals; yield 65%; mp  $151\text{--}152 \text{ }^\circ\text{C}$ . IR ( $\nu_{\text{max}}$ ,  $\text{cm}^{-1}$ ): 3356 (N-H), 2899, 1647 (C=O), 1543 (N-H), 1332, 1165, 1124, 1068.  $^1\text{H}$  NMR (DMSO- $d_6$ ),  $\delta$ , ppm: 1.33–1.69 (m, 12H), 1.85–1.98 (m, 3H), 2.97 (d,  $^3J = 6.2 \text{ Hz}$ , 2H), 7.79 (d,  $^3J = 8.0 \text{ Hz}$ , 2H), 8.00 (d,  $^3J = 8.0 \text{ Hz}$ , 2H), 8.46 (t,  $^3J = 6.2 \text{ Hz}$ , 1H).  $^{13}\text{C}$  NMR ( $\text{CDCl}_3$ ),  $\delta$ , ppm: 28.25, 34.14, 36.95, 40.41, 51.61, 123.76 (q,  $^1J_{\text{CF}} = 270.8 \text{ Hz}$ ), 125.74 (q,  $^3J_{\text{CF}} = 3.8 \text{ Hz}$ ), 127.43, 133.14 (q,  $^2J_{\text{CF}} = 32.6 \text{ Hz}$ ), 138.40, 166.59. MS,  $m/z$  (%): 337 ( $\text{M}^+$ , 22), 318 (2), 173 (12), 145 (10), 135 (100), 107 (6), 93 (10), 79 (10). EA calcd. for  $\text{C}_{19}\text{H}_{22}\text{F}_3\text{NO}$ : C 67.64, H 6.57, N 4.15; found: C 67.61, H 6.63, N 4.12.

*N*-((Adamantan-1-yl)methyl)-4-bromobenzamide (**9**). Colorless crystals; yield 64%; mp  $190\text{--}192 \text{ }^\circ\text{C}$ . IR ( $\nu_{\text{max}}$ ,  $\text{cm}^{-1}$ ): 3269 (N-H), 2902, 1631 (C=O), 1589, 1548, 1309, 1068, 1010.  $^1\text{H}$  NMR (DMSO- $d_6$ ),  $\delta$ , ppm: 1.45–1.82 (m, 12H), 1.85–1.98 (m, 3H), 2.97 (d,  $^3J = 6.2 \text{ Hz}$ , 2H), 7.59 (d,  $^3J = 8.0 \text{ Hz}$ , 2H), 7.75 (d,  $^3J = 8.0 \text{ Hz}$ , 2H), 7.95 (br. s, 1H).  $^{13}\text{C}$  NMR (DMSO- $d_6$ ),  $\delta$ , ppm: 28.49, 34.78, 37.22, 40.78, 51.38, 124.95, 129.89, 131.62, 134.96, 166.49. MS,  $m/z$  (%): 347 ( $\text{M}^+$ , 20), 212 (1), 183 (8), 157 (6), 135 (100), 107 (6), 93 (11), 79 (11). EA calcd. for  $\text{C}_{18}\text{H}_{22}\text{BrNO}$ : C 62.08, H 6.37, N 4.02; found: C 61.93, H 6.42, N 4.09.

*N*-(Adamantan-2-yl)-4-bromobenzamide (**11**). Colorless crystals; yield 72%; mp  $181\text{--}182 \text{ }^\circ\text{C}$ . IR ( $\nu_{\text{max}}$ ,  $\text{cm}^{-1}$ ): 3348 (N-H), 2904, 1633 (C=O), 1537 (N-H), 1321, 1105, 1068, 1012.  $^1\text{H}$  NMR (DMSO- $d_6$ ),  $\delta$ , ppm: 1.40–2.15 (m, 14H), 3.92–4.05 (m, 1H), 7.61 (d,  $^3J = 8.5 \text{ Hz}$ , 2H), 7.75 (d,  $^3J = 8.5 \text{ Hz}$ , 2H), 7.96 (d,  $^3J = 6.4 \text{ Hz}$ , 1H).  $^{13}\text{C}$  NMR (DMSO- $d_6$ ),  $\delta$ , ppm: 27.33, 31.61, 31.68, 37.42, 37.69, 54.77, 125.06, 130.35, 131.53, 134.81, 166.16. MS,  $m/z$  (%): 333 ( $\text{M}^+$ , 100), 254 (5), 200 (7), 183 (55), 155 (24), 134 (44), 119 (14), 91 (20), 79 (16). EA calcd. for  $\text{C}_{17}\text{H}_{20}\text{BrNO}$ : C 61.09, H 6.03, N 4.19; found: C 61.13, H 6.10, N 4.14.

*N*-(Adamantan-2-yl)-4-(trifluoromethyl)benzamide (**12**). Colorless crystals; yield 68%; mp  $183\text{--}185 \text{ }^\circ\text{C}$ . IR ( $\nu_{\text{max}}$ ,  $\text{cm}^{-1}$ ): 3334 (N-H), 2904, 1635 (C=O), 1533 (N-H), 1321, 1163, 1105, 1064, 1016.  $^1\text{H}$  NMR (DMSO- $d_6$ ),  $\delta$ , ppm: 1.39–2.12 (m, 14H), 4.00 (m, 1H), 7.78 (d,  $^3J = 8.2 \text{ Hz}$ , 2H), 7.96 (d,  $^3J = 8.2 \text{ Hz}$ , 2H), 8.17 (d, 6.6 Hz, 1H).  $^{13}\text{C}$

NMR (DMSO-*d*<sub>6</sub>),  $\delta$ , ppm: 27.32, 31.61, 31.68, 37.41, 37.69, 54.89, 124.54 (q,  $^1J_{CF}$  = 270.8 Hz), 125.53 (q,  $^3J_{CF}$  = 3.8 Hz), 129.09, 131.31 (q,  $^2J_{CF}$  = 31.4 Hz), 139.68, 166.15. MS, *m/z* (%): 323 (*M*<sup>+</sup>, 55), 304 (7), 280 (2), 266 (2), 207 (7), 173 (100), 145 (71). EA calcd. for C<sub>18</sub>H<sub>20</sub>F<sub>3</sub>N<sub>2</sub>O: C 66.86, H 6.23, N 4.33; found: C 66.81, H 6.30, N 4.28.

*N*<sup>1</sup>-(4-(Trifluoromethyl)benzoyl)adamantane-1-carbohydrazide (**16**). Colorless crystals; yield 63%; mp 227–229 °C; IR ( $\nu_{\max}$ , cm<sup>-1</sup>): 3336 (N-H), 3184 (N-H), 2908, 1631(C=O), 1548, 1514, 1319, 1165, 1128, 1060. <sup>1</sup>H NMR (DMSO-*d*<sub>6</sub>),  $\delta$ , ppm: 1.58–1.89 (m, 12H), 1.93–2.09 (m, 3H), 7.84 (d,  $^3J$  = 8.2 Hz, 2H), 8.03 (d,  $^3J$  = 8.2 Hz, 2H), 9.49 (s, 1H), 10.39 (s, 1H). <sup>13</sup>C NMR (DMSO-*d*<sub>6</sub>),  $\delta$ , ppm: 28.07, 36.60, 39.05, 40.09, 124.41 (q,  $^1J_{CF}$  = 270.7 Hz), 126.09 (q,  $^3J_{CF}$  = 3.8 Hz), 128.81, 132.05 (q,  $^2J_{CF}$  = 32.4 Hz), 137.05, 164.94, 176.81. MS, *m/z* (%): 366 (*M*<sup>+</sup>, 2), 347 (2), 173 (9), 163 (12), 135 (100). EA calcd. for C<sub>19</sub>H<sub>21</sub>F<sub>3</sub>N<sub>2</sub>O<sub>2</sub>: C 62.29, H 5.78, N 7.65; found: C 62.23, H 5.84, N 7.61.

3,5-Dimethyl-*N*<sup>1</sup>-(4-(trifluoromethyl)benzoyl)adamantane-1-carbohydrazide (**17**). Colorless crystals; yield 66%; mp 183–184 °C. IR ( $\nu_{\max}$ , cm<sup>-1</sup>): 3244 (N-H), 2897, 1683 (C=O), 1651 (C=O), 1546 (NH), 1504 (NH), 1325, 1168, 1130, 1064, 1018. <sup>1</sup>H NMR (DMSO-*d*<sub>6</sub>),  $\delta$ , ppm: 0.80 (s, 6H), 1.09–2.10 (m, 13H), 7.84 (d,  $^3J$  = 8.3 Hz, 2H), 8.02 (d,  $^3J$  = 8.3 Hz, 2H), 9.57 (br. s, 1H), 10.36 (br. s, 1H). <sup>13</sup>C NMR (DMSO-*d*<sub>6</sub>),  $\delta$ , ppm: 29.29, 30.96, 31.19, 37.67, 41.99, 42.86, 45.27, 50.76, 124.40 (q,  $^1J_{CF}$  = 271.7 Hz), 126.04 (q,  $^3J_{CF}$  = 3.8 Hz), 128.81, 132.02 (q,  $^2J_{CF}$  = 32.4 Hz), 137.09, 164.87, 176.53. MS, *m/z* (%): 394 (*M*<sup>+</sup>, 1) 376 (2), 191 (4), 173 (7), 163 (100), 145 (6), 107 (22), 91 (4), 79 (3). EA calcd. for C<sub>21</sub>H<sub>25</sub>F<sub>3</sub>N<sub>2</sub>O<sub>2</sub>: C 63.95, H 6.39, N 7.10; found: C 63.86, H 6.42, N 7.03.

3-Ethyl-*N*<sup>1</sup>-(4-(trifluoromethyl)benzoyl)adamantane-1-carbohydrazide (**18**). Colorless crystals; yield 59%; mp 198–200 °C. IR ( $\nu_{\max}$ , cm<sup>-1</sup>): 3350 (N-H), 3190 (N-H), 2900, 1691 (C=O), 1647 (C=O), 1583, 1516, 1317, 1165, 1107, 1064, 1016. <sup>1</sup>H NMR (DMSO-*d*<sub>6</sub>),  $\delta$ , ppm: 0.75 (t,  $^3J$  = 7.5 Hz, 3H), 1.10 (q,  $^3J$  = 7.5 Hz, 2H), 1.31–2.04 (m, 14H), 7.63 (d,  $^3J$  = 8.0 Hz, 2H), 8.04 (d,  $^3J$  = 8.0 Hz, 2H), 9.94 (br. s, 2H). <sup>13</sup>C NMR (DMSO-*d*<sub>6</sub>),  $\delta$ , ppm: 7.38, 28.64, 32.81, 36.33, 36.37, 39.15, 40.79, 41.07, 43.89, 124.92 (q,  $^1J_{CF}$  = 270.7 Hz), 125.00 (q,  $^2J_{CF}$  = 3.8 Hz), 128.21, 129.47 (q,  $^2J_{CF}$  = 32.4 Hz), 141.89, 163.58, 172.49. MS, *m/z* (%): 394 (*M*<sup>+</sup>, 1), 376 (3), 347 (4), 191 (3), 173 (8), 163 (100), 145 (6), 107 (8), 93 (8), 79 (7). EA calcd. for C<sub>21</sub>H<sub>25</sub>F<sub>3</sub>N<sub>2</sub>O<sub>2</sub>: C 63.95, H 6.39, N 7.10; found: C 63.91, H 6.44, N 7.06.

*N*<sup>1</sup>-(Adamantan-1-yl)-2-(4-(trifluoromethyl)benzoyl)hydrazine-1-carboxamide (**20**). Colorless crystals; yield 61%; mp 173–175 °C. IR ( $\nu_{\max}$ , cm<sup>-1</sup>): 3307 (N-H), 2906, 1687, 1641 (C=O), 1552, 1323, 1165, 1128, 1064, 1018. <sup>1</sup>H NMR (DMSO-*d*<sub>6</sub>),  $\delta$ , ppm: 1.46–1.92 (m, 12H), 1.93–2.05 (m, 3H), 5.99 (s, 1H), 7.69 (s, 1H), 7.83 (d,  $^3J$  = 8.2 Hz, 2H), 8.01 (d,  $^3J$  = 8.2 Hz, 2H), 10.29 (s, 1H). <sup>13</sup>C NMR (DMSO-*d*<sub>6</sub>),  $\delta$ , ppm: 29.43, 36.54, 42.26, 50.48, 124.41 (q,  $^1J_{CF}$  = 271.7 Hz), 125.94 (q,  $^3J_{CF}$  = 3.8 Hz), 128.85, 131.95 (q,  $^2J_{CF}$  = 32.4 Hz), 137.09, 157.05, 165.48. MS, *m/z* (%): 381 (*M*<sup>+</sup>, 1), 230 (2), 204 (96), 173 (86), 145 (28), 135 (100), 93 (24), 79 (23). EA calcd. for C<sub>19</sub>H<sub>22</sub>F<sub>3</sub>N<sub>3</sub>O<sub>2</sub>: C 59.83, H 5.81, N 11.02; found: C 59.78, H 5.89, N 10.97.

#### 4.2.3. General procedure for the synthesis of compounds 25, 26, 31

To the solution of hydrazone (**23**, **24**, **30**) (10 mmol) and triethylamine (12 mmol) in 10 ml of methylene chloride a solution of *p*-trifluoromethylbenzoic acid chloride (10 mmol) in 10 ml of methylene chloride was added dropwise under stirring at 10 °C. The reaction mixture was stirred for 3 h at rt. The solvent was evaporated, the precipitate was filtered off, dried and recrystallized from ethanol to give hydrazones (**25**, **26**, **31**) in a yield of 68–69%. The hydrazone (**26**) was subjected to the reduction step without purification.

*N*<sup>1</sup>-(Adamantan-2-ylidene)-4-(trifluoromethyl)benzohydrazide (**25**). Colorless crystals; yield 68%; m.p. 225–227 °C. IR ( $\nu_{\max}$ ,

cm<sup>-1</sup>) = 3150 (N-H), 2908, 1657 (C=N), 1649 (C=O), 1631, 1539 (N-H), 1321, 1168, 1105, 1064, 1018. <sup>1</sup>H NMR (DMSO-*d*<sub>6</sub>),  $\delta$ , ppm: 1.64–2.05 (m, 12H), 2.52–2.66 (m, 1H), 3.15–3.23 (m, 1H), 7.80 (d,  $^3J$  = 8.1 Hz, 2H), 7.96 (d,  $^3J$  = 8.1 Hz, 2H), 10.78 (s, 1H). <sup>13</sup>C NMR (DMSO-*d*<sub>6</sub>),  $\delta$ , ppm: 27.68, 32.3, 36.31, 37.85, 39.19, 39.61, 124.49 (q,  $^1J_{CF}$  = 272.2 Hz), 125.68 (q,  $^3J_{CF}$  = 3.6 Hz), 129.14, 131.51 (q,  $^2J_{CF}$  = 32.6 Hz), 138.66, 163.08, 173.19. MS, *m/z* (%): 336 (65) [*M*]<sup>+</sup>, 307 (10), 265 (12), 190 (62), 173 (100), 145 (46), 163 (36), 137 (10), 91 (22), 79 (21). EA calcd. for C<sub>18</sub>H<sub>19</sub>F<sub>3</sub>N<sub>2</sub>O: C 64.28, H 5.69, N 8.33; found: C 64.23, H 5.77, N 8.27.

*N*<sup>1</sup>-(1-(Adamantan-1-yl)ethylidene)-4-(trifluoromethyl)benzohydrazide (**31**). Colorless crystals; yield 69%; m.p. 213–215 °C. IR ( $\nu_{\max}$ , cm<sup>-1</sup>) = 3280 (NH), 2904, 1659 (C=N), 1651(C=O), 1541 (N-H), 1325, 1128, 1103, 1066. <sup>1</sup>H NMR (DMSO-*d*<sub>6</sub>),  $\delta$ , ppm: 1.45–2.10 (m, 15H), 1.86 (s, 3H), 7.81 (d,  $^3J$  = 7.8 Hz, 2H), 7.97 (d,  $^3J$  = 7.8 Hz, 2H), 10.49 (s, 1H). <sup>13</sup>C NMR (DMSO-*d*<sub>6</sub>),  $\delta$ , ppm: 27.73, 30.81, 31.45, 37.12, 37.93, 124.46 (q,  $^1J_{CF}$  = 271.7 Hz), 125.84 (q,  $^3J_{CF}$  = 3.8 Hz), 128.60, 131.62 (q,  $^2J_{CF}$  = 32.4 Hz), 137.55, 160.46, 164.77. MS, *m/z* (%): 364 (*M*<sup>+</sup>, 1) 345 (2), 229 (100), 173 (13), 145 (10), 135 (3), 91 (5), 79 (5). EA calcd. for C<sub>20</sub>H<sub>23</sub>F<sub>3</sub>N<sub>2</sub>O: C 65.92, H 6.36, N 7.69; found: C 65.87, H 6.41, N 7.65.

#### 4.2.4. General procedure for the synthesis of compounds 27, 28, 32

To the solution of hydrazine (**25**, **26**, **31**) (12 mmol) in 20 mL of methanol 3 mL of glacial acetic acid were added followed by addition of sodium cyanoborohydride (10 mmol). The reaction mixture was then stirred at rt for 24 h. Aqueous NaOH solution (15 mL, 10%) was then added and most of the CH<sub>3</sub>OH was removed on a rotary evaporator. The reaction mixture was diluted with water (30 mL) and the product was extracted with CH<sub>2</sub>Cl<sub>2</sub> (3 × 10 ml). The organic extract was dried with sodium sulfate and evaporated to yield hydrazide (**27**, **28**, **32**).

*N*<sup>1</sup>-(Adamantan-2-yl)-4-(trifluoromethyl)benzohydrazide (**27**). Colorless crystals; yield 83%; mp 218–220 °C. IR ( $\nu_{\max}$ , cm<sup>-1</sup>) = 3296 (NH), 2900, 1633 (C=O), 1533, 1325, 1161, 1128, 1066. <sup>1</sup>H NMR (DMSO-*d*<sub>6</sub>),  $\delta$ , ppm: 1.32–2.26 (m, 14H), 2.99–3.04 (m, 1H), 5.03 (br. s, 1H), 7.77 (d,  $^3J$  = 8.0 Hz, 2H), 7.99 (d,  $^3J$  = 8.0 Hz, 2H), 9.99 (br. s, 1H). <sup>13</sup>C NMR (DMSO-*d*<sub>6</sub>),  $\delta$ , ppm: 27.84, 31.04, 31.56, 37.29, 38.02, 63.74, 124.48 (q,  $^1J_{CF}$  = 270.8 Hz), 125.70 (q,  $^3J_{CF}$  = 3.8 Hz), 128.56, 131.73 (q,  $^2J_{CF}$  = 31.5 Hz), 137.77, 164.81. MS, *m/z* (%): 338 (*M*<sup>+</sup>, 4), 319 (4), 190 (35), 173 (28), 149 (100), 135 (64), 107 (11), 93 (21), 79 (20). EA calcd. for C<sub>18</sub>H<sub>21</sub>F<sub>3</sub>N<sub>2</sub>O: C 63.89, H 6.26, N 8.28; found: C 63.83, H 6.32, N 8.24.

*N*<sup>1</sup>-(5-Chloroadamantan-2-yl)-4-(trifluoromethyl)benzohydrazide (**28**). Colorless crystals; yield 67%; mp 141–142 °C; E:Z = 2:1 (GC-MS). IR ( $\nu_{\max}$ , cm<sup>-1</sup>) = 3298 (NH), 2918, 1633 (C=O), 1537 (NH), 1321, 1163, 1130, 1066; <sup>1</sup>H NMR (DMSO-*d*<sub>6</sub>),  $\delta$ , ppm: 1.29–3.10 (m, 28H, E + Z), 5.11 (d d,  $^3J$  = 3.0 Hz,  $^3J$  = 5.7 Hz) and 5.14 (d d,  $^3J$  = 3.7 Hz,  $^3J$  = 6.0 Hz) (2H, E + Z), 7.78 (d,  $^3J$  = 8.2 Hz, 4H, E + Z), 7.99 (d,  $^3J$  = 8.2 Hz, 4H, E + Z), 10.08 (d,  $^3J$  = 5.7 Hz) and 10.11 (d,  $^3J$  = 6.0 Hz) (2H, E + Z). <sup>13</sup>C NMR (DMSO-*d*<sub>6</sub>),  $\delta$ , ppm: 29.37, 31.29, 33.94, 34.39, 34.65, 41.67, 46.81, 48.03, 48.11, 61.39, 60.69, 69.72, 70.43, 124.48 (q,  $^1J_{CF}$  = 276.1 Hz), 125.90 (q,  $^3J_{CF}$  = 3.8 Hz), 128.65, 131.68 (q,  $^2J_{CF}$  = 31.5 Hz), 137.52, 165.06, 165.31. MS, *m/z* (%): 372 (*M*<sup>+</sup>, 1), 353 (1), 190 (100), 173 (34), 145 (17), 133 (17), 91 (20), 79 (12). EA calcd. for C<sub>18</sub>H<sub>20</sub>ClF<sub>3</sub>N<sub>2</sub>O: C 57.99, H 5.41, N 7.51; found: C 57.91, H 5.48, N 7.47.

(*rac*)-*N*<sup>1</sup>-(1-(Adamantan-1-yl)ethyl)-4-(trifluoromethyl)benzohydrazide (**32**). Colorless crystals; yield 80%; mp 217–219 °C. IR ( $\nu_{\max}$ , cm<sup>-1</sup>) = 3189 (N-H), 2910, 1678 (C=O), 1570, 1541, 1326, 1166, 1126, 1066, 1014. <sup>1</sup>H NMR (DMSO-*d*<sub>6</sub>),  $\delta$ , ppm: 1.11(d,  $^3J$  = 6.9 Hz, 3H), 1.47–1.81 (m, 12H), 1.89–2.05 (m, 3H), 2.86 (q,  $^3J$  = 6.9 Hz, 1H), 6.7 (br. s, 1H), 7.87 (d,  $^3J$  = 8.3 Hz, 2H), 8.09 (d,  $^3J$  = 8.3 Hz, 2H), 11.69 (br. s, 1H). <sup>13</sup>C NMR (DMSO-*d*<sub>6</sub>),  $\delta$ , ppm: 11.36, 28.17, 35.41, 36.85, 38.08, 67.28, 124.33 (q,  $^1J_{CF}$  = 270.8 Hz), 126.08 (q,  $^3J_{CF}$  = 3.8 Hz), 129.24,

132.53 (q,  $^2J_{CF} = 31.4$  Hz), 135.68, 164.63. MS,  $m/z$  (%): 366 ( $M^+$ , 2), 231 (100), 190 (8), 173 (20), 145 (10), 135 (7), 91 (6), 79 (7). EA calcd. for  $C_{20}H_{25}F_3N_2O$ : C 65.56, H 6.88, N 7.65; found: C 65.45, H 6.96, N 7.59.

#### 4.2.5. General procedure for the synthesis of compounds 35, 36

To a solution of 0.70 g adamant-1-ylhydrazine dihydrochloride (**33**) or 3-ethyladamant-1-ylhydrazine dihydrochloride (**34**) (3 mmol) and 0.42 g of sodium hydroxide (10 mmol) in 10 mL of water a solution of 0.6 g (3 mmol) *p*-trifluoromethylbenzoyl chloride in 20 mL of ether was added under stirring at rt during 5 min and the stirring continued for 1 h. The ether layer was separated, washed with 10 ml of water, dried with sodium sulfate and evaporated. The residue was then recrystallized from the mixture of hexane and toluene (1:1) to give the product.

*N*<sup>1</sup>-(Adamantan-1-yl)-4-(trifluoromethyl)benzohydrazide (**35**). Colorless crystals; yield 72%; mp 150–152 °C. IR ( $\nu_{max}$ ,  $cm^{-1}$ ) = 3199 (N-H), 3099 (N-H), 2912, 1658 (C=O), 1585 (N-H), 1311, 1165, 1124, 1060. <sup>1</sup>H NMR (DMSO-*d*<sub>6</sub>),  $\delta$ , ppm: 1.45–1.68 (m, 12H), 1.95–2.05 (m, 3H), 4.91 (s, 1H), 7.81 (d,  $^3J = 8.2$  Hz, 2H), 7.99 (d,  $^3J = 8.2$  Hz, 2H), 9.99 (s, 1H). <sup>13</sup>C NMR (DMSO-*d*<sub>6</sub>),  $\delta$ , ppm: 29.27, 36.64, 41.23, 55.25, 124.47 (q,  $^1J_{CF} = 270.7$  Hz), 125.85 (q,  $^3J_{CF} = 3.8$  Hz), 128.69, 131.58 (q,  $^2J_{CF} = 31.8$  Hz), 137.43, 165.09. MS,  $m/z$  (%): 338 ( $M^+$ , 11), 173 (10), 145 (7), 135 (100), 107 (7), 93 (14), 79 (13). EA calcd. for  $C_{18}H_{21}F_3N_2O$ : C 63.89, H 6.26, N 8.28; found: C 63.81, H 6.32, N 8.22.

*N*<sup>1</sup>-(3-Ethyladamantan-1-yl)-4-(trifluoromethyl)benzohydrazide (**36**). Colorless crystals; yield 74%; mp 133–135 °C. IR ( $\nu_{max}$ ,  $cm^{-1}$ ): 3253 (N-H), 2905, 1666 (C=O), 1581, 1537 (N-H), 1317, 1165, 1124, 1062, 1014. <sup>1</sup>H NMR (DMSO-*d*<sub>6</sub>),  $\delta$ , ppm: 0.72 (t,  $^3J = 7.3$  Hz, 3H), 1.08 (q,  $^3J = 7.3$  Hz, 2H), 1.21–1.61 (m, 12H), 1.99–2.09 (m, 2H), 5.05 (br. s, 1H), 7.80 (d,  $^3J = 8.3$  Hz, 2H), 7.99 (d,  $^3J = 8.3$  Hz, 2H), 9.99 (br. s, 1H). <sup>13</sup>C NMR (DMSO-*d*<sub>6</sub>),  $\delta$ , ppm: 7.56, 29.52, 34.45, 36.08, 36.28, 40.87, 41.06, 45.53, 56.22, 124.46 (q,  $^1J_{CF} = 270.7$  Hz), 125.85 (q,  $^3J_{CF} = 3.8$  Hz), 128.69, 131.61 (q,  $^2J_{CF} = 31.8$  Hz), 137.41, 165.09. MS,  $m/z$  (%): 366 ( $M^+$ , 9), 163 (100), 145 (7), 135 (3), 107 (13), 93 (14), 79 (10). EA calcd. for  $C_{20}H_{25}F_3N_2O$ : C 65.56, H 6.88, N 7.65; found: C 65.49, H 6.95, N 7.63.

#### 4.3. Poxvirus inhibitory activity evaluation

Antiviral activity of compounds **5–9**, **11**, **12**, **16–18**, **20**, **25**, **27**, **28**, **31**, **32**, **35–38** against orthopoxviruses was determined *in vitro* in Vero cell culture. Vero cell monolayer was grown in DMEM (Biolot, Russia) in the presence of 5% fetal bovine serum (HyClone, USA) with the addition of gentamicin sulfate (40 units/ml) and amphotericin B (2.5 units/ml) The same medium was used as a support for the cultivation of cells with the virus, but with the addition of 2% serum.

Vaccinia virus (strain Copenhagen), cowpox virus (strain Grishak), mousepox virus - ectromelia (strain K-1), obtained from the State collection of pathogens of viral infections and rickettsioses of SRC VB Vector (Koltsovo, Novosibirsk region, Russia) were used in the work. Viruses were produced in Vero cell culture in DMEM medium (Biolot, Russia). The concentration of viruses in the culture fluid was determined by the method of plaques by titration of samples in a culture of Vero cells, calculated and expressed in decimal logarithms of plaque-forming units per ml (lg PFU/ml) [63]. The virus concentration in the samples used in the work was  $6.85 \pm 0.50$  lg PFU/ml. The accumulated and used in work series of viruses with the indicated titer were stored at  $-70^\circ\text{C}$ .

Compound 4-trifluoromethyl-N-(3,3a,4,4a,5,5a,6,6a-octahydro-1,3-dioxo-4,6-ethenocycloprop(f)isoindol-2(1H)-yl)-benzamide (tecovirimat), synthesized in N.N. Vorozhtsov Novosibirsk Institute of Organic Chemistry, Siberian Branch of the Russian Academy

according to the method described by the authors [64], was used as a reference compound.

Evaluation of antiviral efficacy of the compounds was carried out according to an adapted and modified method [65]. To assess the effectiveness of each sample 8 three-fold dilutions were used. The initial concentration of each compound was 1, 10 or 100  $\mu\text{g/ml}$ , depending on the preliminary screening of antiviral activity and toxicity of the drug. For evaluating the antiviral activity firstly to the wells of 96-well plates with a monolayer of cells containing 100  $\mu\text{l}$  of DMEM medium with 2% fetal serum of a 50- $\mu\text{l}$  dilution of the samples were added, and then 50  $\mu\text{l}$  of a 1000 pfu/well virus dose was added. Evaluation of antiviral activity was performed after 4 days. After incubation of the cell monolayers infected with orthopoxvirus and treated with tested compounds for 4 days, a vital red dye “neutral red” was added to the culture medium for 1.5 h. Next, the monolayer was washed twice with saline solution, the lysis buffer was added and after 30 min the optical density (OD), which is an indicator of the number of cells in the monolayer that is not destroyed under the influence of virus, was measured on an Emax plate reader (Molecular Devices, USA). The OD values were used to calculate a 50% cytotoxic concentration ( $CC_{50}$   $\mu\text{M}$ ) and a 50% virus inhibiting concentration ( $IC_{50}$   $\mu\text{M}$ ) using the SoftMax Pro-4.0 computer program. Based on these indicators, the therapeutic index (TI) (or selectivity index - SI) was calculated:  $SI = CC_{50}/IC_{50}$ . The results of experimental evaluation of antiorthopox activity are represented in Table 1.

#### Declaration of competing interest

The authors declare that they have no known competing financial interests or personal relationships that could have appeared to influence the work reported in this paper.

#### Acknowledgement

The authors gratefully acknowledge the support of this work by the Russian Science Foundation (project 20-73-00254) for synthesis of compounds and Russian Ministry of Education and Science for a basic part of a research project 0778-2020-0005 for investigation of properties of synthesized compounds with the use of scientific equipment of the Center for Collective Use “Investigation of the Physicochemical properties of Substances and Materials”.

#### Appendix A. Supplementary data

Supplementary data to this article can be found online at <https://doi.org/10.1016/j.ejmech.2021.113485>.

#### References

- [1] N. Sklenovská, M. Van Ranst, Emergence of monkeypox as the most important orthopoxvirus infection in humans, *Front Public Health* 6 (2018) 241, <https://doi.org/10.3389/fpubh.2018.00241>.
- [2] D. DiEuliis, K. Berger, G. Gronvall, Biosecurity implications for the synthesis of horsepox, an orthopoxvirus, *Health Security* (5) (2017) 629–637, <https://doi.org/10.1089/hs.2017.0081>, 016.
- [3] S.N. Shchelkunov, An increasing danger of zoonotic orthopoxvirus infections, *PLoS Pathog.* 9 (12) (2013), <https://doi.org/10.1371/journal.ppat.1003756> e1003756.
- [4] G. Bohelay, T.-A. Duong, Infections humaines à poxvirus, *Ann. Dermatol. Venerol.* 146 (5) (2019) 387–398, <https://doi.org/10.1016/j.jannder.2019.03.001>.
- [5] S. Sarker, C. Hannon, A. Athukorala, H. Bielefeldt-Ohmann, Emergence of a novel pathogenic poxvirus infection in the endangered green sea turtle (*Chelonia mydas*) highlights a key threatening process, *Viruses* 13 (2) (2021) 219, <https://doi.org/10.3390/v13020219>.
- [6] R.C. Hendrickson, C. Wang, E.L. Hatcher, E.J. Lefkowitz, Orthopoxvirus genome evolution: the role of gene loss, *Viruses* 2 (9) (2010) 1933–1967, <https://doi.org/10.3390/v2091933>.



- [7] G. Impelluso, F. Lentzos, The threat of synthetic smallpox: European perspectives, *Health Security* 16 (5) (2017) 582–586, <https://doi.org/10.1089/hs.2017.0045>.
- [8] R.S. Noyce, S. Lederman, D.H. Evans, Construction of an infectious horsepox virus vaccine from chemically synthesized DNA fragments, *PLoS* 13 (1) (2018), <https://doi.org/10.1371/journal.pone.0188453> e0188453.
- [9] B. Moss, Poxvirus DNA replication, *Cold Spring Harb Perspect Biol* 5 (9) (2013), <https://doi.org/10.1101/cshperspect.a010199> a010199.
- [10] S.N. Shchelkunov, Orthopoxvirus genes that mediate disease virulence and host tropism, *Advanc Virol ID* (2012), 524743, <https://doi.org/10.1155/2012/524743>.
- [11] G. Andrei, R. Snoeck, Cidofovir activity against poxvirus infections, *Viruses* 2 (12) (2010) 2803–2830, <https://doi.org/10.3390/v2122803>.
- [12] A.S. Sokolova, K.S. Kovaleva, O.I. Yarovaya, N.I. Bormotov, L.N. Shishkina, O.A. Serova, A.A. Sergeev, A.P. Agafonov, R.A. Maksuytov, N.F. Salakhutdinov, (+)-Campthor and (–)-borneol derivatives as potential anti-orthopoxvirus agents, *Arch Pharm* (2021), <https://doi.org/10.1002/ardp.202100038> e2100038.
- [13] M.N. Prichard, E.R. Kern, Orthopoxvirus targets for the development of new antiviral agents, *Antivir. Res.* 94 (2) (2012) 111–125, <https://doi.org/10.1016/j.antiviral.2012.02.012>.
- [14] Y.N. Klimochkin, V.A. Shiryayev, M.V. Leonova, Antiviral properties of cage compounds. New prospects, *Russ. Chem. Bull.* 64 (7) (2015) 1473–1496, <https://doi.org/10.1007/s11172-015-1035-y>.
- [15] I.K. Moiseev, S.A. Kon'kov, K.A. Ovchinnikov, N.M. Kilyaeva, K.M. Bormasheva, O.N. Nechaeva, M.V. Leonova, Y.N. Klimochkin, S.M. Balachin, N.I. Bormotov, O.A. Serova, E.F. Belanov, Synthesis and antiviral activity of new adamantane derivatives, *Pharm. Chem. J.* 45 (10) (2012) 588–592, <https://doi.org/10.1007/s11094-012-0686-3>.
- [16] Y.N. Klimochkin, M.V. Leonova, I.R. Korzhev, I.K. Moiseev, G.V. Vladyko, L.V. Korobchenko, E.I. Boreko, S.N. Nikolaeva, Antiviral activity of adamantane series hydroxy derivatives, *Pharm. Chem. J.* 26 (7–8) (1992) 616–618, <https://doi.org/10.1007/BF00777145>.
- [17] N. Kolocouris, A. Kolocouris, G.B. Foscolos, G. Fytas, J. Neyts, E. Padalko, J. Balzarini, R. Snoeck, G. Andrei, E. De Clercq, Synthesis and antiviral activity evaluation of some new aminoadamantane derivatives, *J. Med. Chem.* 39 (17) (1996) 3307–3318, <https://doi.org/10.1021/jm950891z>.
- [18] Klimochkin YuN, I.K. Moiseev, G.V. Vladyko, L.V. Korobchenko, E.I. Boreko, Synthesis and investigation of viral-inhibitory activity of nitrogen-containing derivatives of adamantane, *Pharm. Chem. J.* 25 (7) (1991) 485–488, <https://doi.org/10.1007/BF00772005>.
- [19] Klimochkin YuN, I.K. Moiseev, O.V. Abramov, G.V. Vladyko, L.V. Korobchenko, E.I. Boreko, Synthesis and antiviral activity of sulfur-containing derivatives of adamantane, *Pharm. Chem. J.* 25 (7) (1991) 489–492, <https://doi.org/10.1007/BF00772006>.
- [20] Y.N. Klimochkin, I.K. Moiseev, E.I. Boreko, G.V. Vladyko, L.V. Korobchenko, Synthesis and antiviral activity of nitrogen-containing adamantane derivatives, *Pharm. Chem. J.* 23 (4) (1989) 304–307, <https://doi.org/10.1007/BF00758419>.
- [21] A. Kolocouris, K. Dimas, C. Pannecouque, M. Witvrouw, G.B. Foscolos, G. Stamatou, G. Fytas, G. Zoidis, N. Kolocouris, G. Andrei, R. Snoeck, E. De Clercq, New 2-(1-adamantylcarbonyl)pyridine and 1-acetyladamantane thiosemicarbazones–thiocarbonohydrazones: cell growth inhibitory, antiviral and antimicrobial activity evaluation, *Bioorg. Med. Chem. Lett* 12 (5) (2002) 723–727, [https://doi.org/10.1016/S0960-894X\(01\)00838-1](https://doi.org/10.1016/S0960-894X(01)00838-1).
- [22] H. Banie, A. Sinha, R.J. Thomas, J.C. Sircar, M.L. Richards, 2-Phenylimidazopyridines, a new series of golgi compounds with potent antiviral activity, *J. Med. Chem.* 50 (24) (2007) 5984–5993, <https://doi.org/10.1021/jm0704907>.
- [23] E.V. Suslov, E.S. Mozhaytsev, D.V. Korchagina, N.I. Bormotov, O.I. Yarovaya, K.P. Volcho, O.A. Serova, A.P. Agafonov, R.A. Maksuytov, L.N. Shishkina, N.F. Salakhutdinov, New chemical agents based on adamantane–monoterpene conjugates against orthopoxvirus infections, *RSC Med Chem* 11 (2020) 1185–1195, <https://doi.org/10.1039/d0md00108b>.
- [24] T.R. Bailey, S.R. Rippin, E. Opsitnick, C.J. Burns, D.C. Pevear, M.S. Collett, G. Rhodes, S. Tohan, J.W. Huggins, R.O. Baker, E.R. Kern, K.A. Keith, D. Dai, G. Yang, D. Hraby, R. Jordan, N-(3,3a,4,4a,5,5a,6,6a-Octahydro-1,3-dioxo-4,6-ethenocycloprop[flisoindol-2-(1H)-yl]carbox-amides: identification of novel orthopoxvirus egress inhibitors, *J. Med. Chem.* 50 (7) (2007) 1442–1444, <https://doi.org/10.1021/jm061484y>.
- [25] G. Yang, D.C. Pevear, M.H. Davies, M.S. Collett, T. Bailey, S. Rippen, L. Barone, C. Burns, G. Rhodes, S. Tohan, J.W. Huggins, R.O. Baker, R.L. Buller, E. Touchette, K. Waller, J. Schriewer, J. Neyts, E. DeClercq, K. Jones, D. Hraby, R. Jordan, An orally bioavailable antipoxvirus compound (ST-246) inhibits extracellular virus formation and protects mice from lethal orthopoxvirus challenge, *J. Virol.* 79 (20) (2005) 13139–13149, <https://doi.org/10.1128/JVI.79.20.13139-13149.2005>.
- [26] D.W. Grosenbach, R. Jordan, D.E. Hraby, Development of the small-molecule antiviral ST-246® as a smallpox therapeutic, *Future Virol.* 6 (5) (2011) 653–671, <https://doi.org/10.2217/fvl.11.27>.
- [27] M. Merchlinsky, A. Albright, V. Olson, H. Schiltz, T. Merkeley, C. Hughes, B. Petersen, M. Challberg, The development and approval of tecovirimat (TPOXX®), the first antiviral against smallpox, *Antivir. Res.* 168 (2019) 168–174, <https://doi.org/10.1016/j.antiviral.2019.06.005>.
- [28] M. Husain, A. Weisberg, B. Moss, Topology of epitope-tagged F13L protein, a major membrane component of extracellular vaccinia virions, *Virology* 308 (2) (2003) 233–242, [https://doi.org/10.1016/S0042-6822\(03\)00063-1](https://doi.org/10.1016/S0042-6822(03)00063-1).
- [29] Duraffour S, Lorenzo MM, Zöller G, Topalis D, Grosenbach D, Hraby DE, Andrei G, Blasco R, Meyer H, Snoeck R. ST-246 is a key antiviral to inhibit the viral F13L phospholipase, one of the essential proteins for orthopoxvirus wrapping. *J Antimicrob Ther* 70(5):1367-1380. doi: 10.1093/jac/dku545.
- [30] S.H. Baek, J.Y. Kwak, S.H. Lee, T. Lee, S.H. Ryu, D.J. Uhlinger, J.D. Lambeth, Lipase activities of p37, the major envelope protein of vaccinia virus, *J. Biol. Chem.* 272 (1997) 32042–32049, <https://doi.org/10.1074/jbc.272.51.32042>.
- [31] G. Hiller, H. Eibl, K. Weber, Characterization of intracellular and extracellular vaccinia virus variants: N1-isonicotinoyl-N2-3-methyl-4-chlorobenzoylhydrazine interferes with cytoplasmic virus dissemination and release, *J. Virol.* 39 (3) (1981) 903–913, <https://jvi.asm.org/content/39/3/903.long>.
- [32] T.C. Sung, R.L. Roper, Y. Zhang, S.A. Rudge, R. Ternel, S.M. Hammond, A.J. Morris, B. Moss, J. Engebrecht, M.A. Frohman, Mutagenesis of phospholipase D defines a superfamily including a trans-Golgi viral protein required for poxvirus pathogenicity, *EMBO J.* 16 (1997) 4519–4530, <https://doi.org/10.1093/emboj/16.15.4519>.
- [33] Y. Chen, K.M. Honeychurch, G. Yang, C.M. Byrd, C. Harver, D.E. Hraby, R. Jordan, Vaccinia virus p37 interacts with host proteins associated with LE-derived transport vesicle biogenesis, *Virol. J.* 6 (2009) 44, <https://doi.org/10.1186/1743-422X-6-44>.
- [34] FDA Advisory Committee Briefing Document, Tecovirimat for the Treatment of Smallpox Disease, Antimicrobial Division Advisory Committee Meeting, May 1, 2018. <https://www.fda.gov/media/112808/download>.
- [35] Y.N. Klimochkin, V.A. Shiryayev, P.V. Petrov, E.V. Radchenko, V.A. Palyulin, N.S. Zefirov, Design of broad-spectrum inhibitors of influenza A virus M2 proton channels: a molecular modeling approach, *Curr. Comput. Aided Drug Des.* 12 (2) (2016) 154–164, <https://doi.org/10.2174/1573409912666160505113408>.
- [36] V.A. Shiryayev, E.V. Radchenko, V.A. Palyulin, N.S. Zefirov, N.I. Bormotov, O.A. Serova, L.N. Shishkina, M.R. Baimuratov, K.M. Bormasheva, Y.A. Guzd, E.A. Ivleva, M.V. Leonova, A.V. Lukashenko, D.V. Osipov, V.A. Osyannin, A.N. Reznikov, V.A. Shadrakova, A.E. Sibiryakova, Y.N. Klimochkin, Molecular design, synthesis and biological evaluation of cage compound-based inhibitors of hepatitis C virus p7 ion channels, *Eur. J. Med. Chem.* 158 (2018) 214–235, <https://doi.org/10.1016/j.ejmech.2018.08.009>.
- [37] W. Yu, A.D. MacKerell, Computer-aided drug design methods, in: P. Sass (Ed.), *Antibiotics. Methods in Molecular Biology* vol. 1520, Humana Press, New York, NY, 2017, [https://doi.org/10.1007/978-1-4939-6634-9\\_5](https://doi.org/10.1007/978-1-4939-6634-9_5).
- [38] J. Yang, R. Yan, A. Roy, D. Xu, J. Poisson, Y. Zhang, The I-TASSER Suite: protein structure and function prediction, *Nat. Methods* 12 (2015) 7–8, <https://doi.org/10.1038/nmeth.3213>.
- [39] A. Roy, A. Kucukural, Y. Zhang, I-TASSER: a unified platform for automated protein structure and function prediction, *Nat. Protoc.* 5 (2010) 725–738, <https://doi.org/10.1038/nprot.2010.5>.
- [40] Y. Zhang, I-TASSER server for protein 3D structure prediction, *BMC Bioinf.* 9 (2008) 40, <https://doi.org/10.1186/1471-2105-9-40>.
- [41] J. Lee, X. Cheng, J.M. Swails, M.S. Yeom, P.K. Eastman, J.A. Lemkul, S. Wei, J. Buckner, J.C. Jeong, Y. Qi, S. Jo, V.P. Pande, D.A. Case, C.L. Brooks, A.D. MacKerell, J.B. Klauda, W. Im, CHARMM-GUI input generator for NAMD, GROMACS, AMBER, OpenMM, and CHARMM/OpenMM simulations using the CHARMM36 additive force field, *J. Chem. Theor. Comput.* 12 (1) (2016) 405–413, <https://doi.org/10.1021/acs.jctc.5b00935>.
- [42] S. Jo, T. Kim, V.G. Iyer, W. Im, CHARMM-GUI: a Web-based graphical user interface for CHARMM, *J. Comput. Chem.* 29 (11) (2008) 1859–1865, <https://doi.org/10.1002/jcc.20945>.
- [43] E.L. Wu, X. Cheng, S. Jo, H. Rui, K.C. Song, E.M. Dávila-Contreras, Y. Qi, J. Lee, V. Monje-Galvan, R.M. Venable, J.B. Klauda, W. Im, CHARMM-GUI Membrane Builder toward realistic biological membrane simulations, *J. Comput. Chem.* 35 (27) (2014) 1997–2004, <https://doi.org/10.1002/jcc.23702>.
- [44] P. Bryk, M.G. Brewer, B.M. Ward, Vaccinia virus phospholipase protein F13 promotes rapid entry of extracellular virions into cells, *J. Virol.* 92 (2018), <https://doi.org/10.1128/JVI.02154-17.e02154-17>.
- [45] J.C. Phillips, R. Braun, W. Wang, J. Gumbart, E. Tajkhorshid, E. Villa, C. Chipot, R.D. Skeel, L. Kale, K. Schulten, Scalable molecular dynamics with NAMD, *J. Comput. Chem.* 26 (2005) 1781–1802, <https://doi.org/10.1002/jcc.20289>.
- [46] E.F. Pettersen, T.D. Goddar, C.C. Huang, G.S. Couch, D.M. Greenblatt, E.C. Meng, T.E. Ferrin, UCSF Chimera—a visualization system for exploratory research and analysis, *J. Comput. Chem.* 25 (13) (2004) 1605–1612, <https://doi.org/10.1002/jcc.20084>.
- [47] Bowie Ju, R. Luthy, D. Eisenberg, A method to identify protein sequences that fold into a known three-dimensional structure, *Science* 253 (5016) (1991) 164–170, <https://doi.org/10.1126/science.1853201>.
- [48] McDermott M, Wakelam MJO, Morris AJ. Phospholipase D. *Biochem. Cell. Biol.* 82:225-253. doi: 10.1139/o03-079.
- [49] Trott O, Olson AJ. AutoDock Vina: improving the speed and accuracy of docking with a new scoring function, efficient optimization and multi-threading. *J. Comput. Chem.* 31(2):455-461. doi: 10.1002/jcc.21334.
- [50] R. Jordan, J.M. Leeds, S. Tyavanagimatt, D.E. Hraby, Development of ST-246 for treatment of poxvirus infections, *Viruses* 2 (2010) 2409–2435, <https://doi.org/10.3390/v2112409>.
- [51] AcD ChemSketch 2015, Advanced Chemistry Development, Inc., Toronto, Canada, 2015. [www.acdlabs.com](http://www.acdlabs.com).

- [52] M.D. Hanwell, D.E. Curtis, D.C. Lonie, T. Vandermeersch, E. Zurek, G.R. Hutchison, Avogadro: an advanced semantic chemical editor, visualization, and analysis platform, *J. Cheminf.* 4 (1) (2012) 17, <https://doi.org/10.1186/1758-2946-4-17>.
- [53] Dassault Systèmes Biovia, *Discovery Studio Visualiser Free, v19.1.0.18287, Dassault Systèmes, San Diego, 2019.*
- [54] D. Schneidman-Duhovny, O. Dror, Y. Inbar, R. Nussinov, H.J. Wolfson, Deterministic pharmacophore detection via multiple flexible alignment of drug-like molecules, *J. Comput. Biol.* 15 (7) (2007) 737–754, <https://doi.org/10.1089/cmb.2007.0130>.
- [55] D. Schneidman-Duhovny, O. Dror, Y. Inbar, R. Nussinov, H.J. Wolfson, PharmaGist: a webserver for ligand-based pharmacophore detection, *Nucleic Acids Res.* 36 (2008) W223–W228, <https://doi.org/10.1093/nar/gkn187>.
- [56] J. Huang, A.D. MacKerell, CHARMM36 all-atom additive protein force field: validation based on comparison to NMR data, *J. Comput. Chem.* 34 (25) (2013) 2135–2145, <https://doi.org/10.1002/jcc.23354>.
- [57] J.B. Klauda, R.M. Venable, J.A. Freites, J.W. O'Connor, D.J. Tobias, C. Mondragon-Ramirez, I. Vorobyov, A.D. MacKerell, R.W. Pastor, Update of the CHARMM all-atom additive force field for lipids: validation on six lipid types, *J. Phys. Chem. B* 114 (23) (2010) 7830–7843, <https://doi.org/10.1021/jp101759q>.
- [58] S. Forli, R. Huey, M.E. Pique, M.F. Sanner, D.S. Goodsell, A.J. Olson, Computational protein-ligand docking and virtual drug screening with the AutoDock suite, *Nat. Protoc.* 11 (5) (2016) 905–919, <https://doi.org/10.1038/nprot.2016.051>.
- [59] G.M. Morris, R. Huey, W. Lindstrom, M.F. Sanner, R.K. Belew, D.S. Goodsell, A.J. Olson, Autodock4 and AutoDockTools4: automated docking with selective receptor flexibility, *J. Comput. Chem.* 30 (16) (2009) 2785–2791, <https://doi.org/10.1002/jcc.21256>.
- [60] T.L. Thomas, M. Fedorchuk, B.V. Shetty, F.E. Anderson, Synthesis and activity of some 3-substituted 1,2,3,4-pseudoxatriazol-5-ones and their precursors and related compounds, *J. Med. Chem.* 13 (2) (1970) 196–203, <https://doi.org/10.1021/jm00296a007>.
- [61] A. Spasov, P.M. Vasil'ev, D.A. Babkov, Prokhorova TYu, E.A. Sturova, Klimochkin YuN, M.V. Leonova, M.R. Baimuratov, New dipeptidyl peptidase 4 inhibitors among adamantane derivatives, *Russ. J. Bioorg. Chem.* 43 (4) (2017) 449–455, <https://doi.org/10.1134/S1068162017040124>.
- [62] P. Mampuy, E. Ruijter, R.V.A. Orru, B.U.W. Maes, Synthesis of secondary amides from thiocarbamates, *Org. Lett.* 20 (14) (2018) 4235–4239, <https://doi.org/10.1021/acs.orglett.8b01654>.
- [63] Brian W.J. Mahy, Hillar O. Kangro (Eds.), *Virology Methods Manual, Academic Press, 1996, p. 374.*
- [64] Mazurkov OYu, A.S. Kabanov, L.N. Shishkina, A.A. Sergeev, M.O. Skarnovich, N.I. Bormotov, M.A. Skarnovich, A.S. Ovchinnikova, K.A. Titova, D.O. Galahova, L.E. Bulychev, ArA. Sergeev, O.S. Taranov, B.A. Selivanov, Tikhonov AYa, E.L. Zavjalov, A.P. Agafonov, A.N. Sergeev, The new effective chemically synthesized anti smallpox compound NIOCH-14, *J. Gen. Virol.* 97 (5) (2016) 1229–1239, <https://doi.org/10.1099/jgv.0.000422>.
- [65] R.O. Baker, M. Bray, J.W. Huggins, Potential antiviral therapeutics for smallpox, monkeypox and other orthopoxvirus infections, *Antivir. Res.* 57 (1–2) (2003) 13–23, [https://doi.org/10.1016/S0166-3542\(02\)00196-1](https://doi.org/10.1016/S0166-3542(02)00196-1).